

ORIGINAL ARTICLE

Open Access



Centimeter-level-precision seafloor geodetic positioning model with self-structured empirical sound speed profile

Shuqiang Xue^{1,2*} , Baojin Li¹, Zhen Xiao^{1,2}, Yue Sun^{1,2} and Jingsen Li³

Abstract

In-field Sound Speed Profile (SSP) measurement is still indispensable for achieving centimeter-level-precision Global Navigation Satellite System (GNSS)-Acoustic (GNSS-A) positioning in current state of the art. However, in-field SSP measurement on the one hand causes a huge cost and on the other hand prevents GNSS-A from global seafloor geodesy especially for real-time applications. We propose an Empirical Sound Speed Profile (ESSP) model with three unknown temperature parameters jointly estimated with the seafloor geodetic station coordinates, which is called the 1st-level optimization. Furthermore, regarding the sound speed variations of ESSP we propose a so-called 2nd-level optimization to achieve the centimeter-level-precision positioning for monitoring the seafloor tectonic movement. Long-term seafloor geodetic data analysis shows that, the proposed two-level optimization approach can achieve almost the same positioning result with that based on the in-field SSP. The influence of substituting the in-field SSP with ESSP on the horizontal coordinates is less than 3 mm, while that on the vertical coordinate is only 2–3 cm in the standard deviation sense.

Keywords GNSS-A, Seafloor geodetic positioning, Sound speed, SSP, Inversion

Introduction

Global Navigation Satellite System (GNSS)-Acoustic (GNSS-A) positioning technique has become a vital tool for seafloor geodesy and crustal deformation applications of submarine offshore regions (Bürgmann & Chadwell, 2014; Iinuma et al., 2021). GNSS-A positioning technique was pioneered by Fred Spiess (Spiess, 1985; Spiess et al., 1998) and further developed for more than two decades (Chadwell & Sweeney, 2010; Chadwell et al., 1997). Regional seafloor geodetic networks were established in the past (Poutanen & Rózsa, 2020; Yang et al., 2020) and

had provided key observations for constraining tectonic motion, crustal deformation and the earthquake cycle (Gagnon & Chadwell, 2007; Gagnon et al., 2005; Iinuma et al., 2021; Kido et al., 2006; Sato et al., 2011). GNSS-A technique achievements made in the past are on the one hand from observation scheme advances (Kido et al., 2008; Sato et al., 2013; Spiess et al., 1998) and on the other hand from acoustic positioning model improvements (Asada & Yabuki, 2006; Fujita et al., 2006; Spiess, 1980; Watanabe et al., 2020; Yang & Qin, 2020; Yokota et al., 2019). Nowadays, terrestrial geodesy has greatly facilitated low-cost and real-time positioning and near-real-time atmosphere state sensing due to positioning model advances (Torge & Müller, 2012), but this has not been achieved in seafloor geodesy. One of important reasons for this is that the high-precision seafloor geodetic positioning seriously relies on the Sound Speed Profile (SSP) measurement in field.

*Correspondence:

Shuqiang Xue
xuesq@casm.ac.cn

¹ Chinese Academy of Surveying and Mapping, Beijing 100830, China

² School of Civil and Architectural Engineering, Shandong University of Technology, Zibo 255049, China

³ College of Geodesy and Geomatics, Shandong University of Science and Technology, Qingdao 266510, China



© The Author(s) 2023. **Open Access** This article is licensed under a Creative Commons Attribution 4.0 International License, which permits use, sharing, adaptation, distribution and reproduction in any medium or format, as long as you give appropriate credit to the original author(s) and the source, provide a link to the Creative Commons licence, and indicate if changes were made. The images or other third party material in this article are included in the article's Creative Commons licence, unless indicated otherwise in a credit line to the material. If material is not included in the article's Creative Commons licence and your intended use is not permitted by statutory regulation or exceeds the permitted use, you will need to obtain permission directly from the copyright holder. To view a copy of this licence, visit <http://creativecommons.org/licenses/by/4.0/>.

The sound speed structure of the ocean water prominently varies from the depth, spatial location and the time (Yokota et al., 2022). Although several global ocean environment observation plans have been in operation (Hayes et al., 1991; Stammer et al., 2003; Zeng et al., 2016), e.g., Array for Real-time Geostrophic Oceanography (Argo) and Transparent Ocean Plan (TOP) (Wu et al., 2020), the current resolution of ocean environment observations, e.g., the Argo observations having a temporal resolution of several days (Roemmich et al., 2009), cannot satisfy the high-precision seafloor geodetic positioning demands; and therefore an in-field Reference SSP (RSSP) measurement is still required. The sound speed can be directly measured or derived from the Conductivity-Temperature-Depth (CTD) profiler measurement (Wilson & Wayne, 1960). However, it is still unrealistic to conduct a high-resolution Sound Speed Field (SSF) measurement for GNSS-A positioning because of the huge cost; and therefore GNSS-A positioning technique in the current state of the art adopts a RSSP to perform the seafloor geodetic positioning (Watanabe et al., 2020). For this, the positioning model requires a strong resist ability to remedy the sound speed variation effect of the RSSP.

The acoustic positioning is seriously affected by the sound speed variations (Kido et al., 2008), which is very familiar to the atmosphere variation affecting GNSS positioning (Chen & Herring, 1997). Inspired by this, the Nadir Total Delay (NTD) model which is analogous to the zenith total delay in GNSS was proposed recently (Honsho & Kido, 2017; Honsho et al., 2019). This idea developed in the GNSS-A positioning can be also found in analyzing the sound speed variation for GNSS-A measurements (Kido et al., 2008). Besides NTD model, a generalized GNSS-A positioning model was also developed to correct the effect of the sound speed variation (Watanabe et al., 2020; Yokota et al., 2022). However, this kind of methods can extract only the sound speed variation relative to the in-field SSP.

In fact, the sound speed variation effect was very early studied by the GNSS-A and SSP observations in Hawaii (Osada et al., 2003). Then, the temporal variation inversion based on the RSSP was developed to eliminate this kind of effect (Fujita et al., 2004, 2006; Matsumoto et al., 2008). For more precisely characterizing the sound speed variation, the inversion method based on a 3-order B-spline model was developed in the past (Ikuta et al., 2008), and then Yokota et al. (2019) advanced this method by extracting the first-order and second-order horizontal sound speed gradients to represent more sound speed variation details (Yasuda et al., 2017). Note that, the above-mentioned inversion methods are based on the RSSP. In fact, the sound speed inversion without

using the RSSP was also developed in the past (Chen, 2014). Recently, a self-constraint positioning method without the assistance of in-field SSP has also been developed (Zhao et al., 2022). However, without using the in-field SSP it is still hard to achieve a desirable positioning accuracy, e.g., the positioning error of the above self-constraint positioning method is up to 0.54 m. Precise positioning models without the assistance of in-field SSP still need to be developed to reduce the in-field SSP measurement cost, which is the vitally meaningful not only for facilitating the low-cost large-scale and even global seafloor geodesy but also for achieving the real-time seafloor geodetic applications, like nowadays mature GNSS geodesy.

This contribution is to develop a Self-structured Empirical SSP (SESSP) approach to achieve centimeter-precision-level seafloor geodetic three-dimensional positioning. In "Three-parameter empirical SSP" section, a three-parameter Empirical Temperature Profile (ETP) model is proposed to structure an Empirical Sound Speed Profile (ESSP) by using the Del Grosso's sound speed formula. In "Two-level optimizations on ESSP" section, a novel GNSS-A positioning model based two-level optimizations is proposed, of which the 1st-level optimization is to fix the ETP model parameters, and the 2nd-level optimization is to finally achieve high-precision location regarding the sound speed variations relative to ESSP. In "Experiment results and tests" section, the proposed models are verified by the long-term seafloor geodetic array observations.

Three-parameter empirical SSP

The horizontal sound speed stratification can be expressed as an exponential SSP with unknowns for applying much of the World's oceans (Munk, 1974). Besides, an empirical bilinear SSP $c_{BP}(u, \mathbf{p}_{BP})$ with four unknown parameters was also proposed and applied in the seafloor geodetic positioning, that is Chen (2014)

$$c_{BP}(u, \mathbf{p}_{BP}) = \begin{cases} v_s + g_u u & 0 \leq u < u_b \\ v_b + g_d(u - u_b) & u_b \leq u \end{cases} \quad (1)$$

where u is the depth, $\mathbf{p}_{BP} = (v_s \ g_u \ g_d \ u_b)$ is the unknown parameter vector, v_s is the surface sound speed, u_b is the bilinear break depth, v_b is the sound speed corresponding to the depth u_b , and g_u and g_d are the piecewise gradients of the bilinear function. The unknown parameters can be estimated jointly with the seafloor geodetic station coordinates.

Chen (2014) pointed out that v_s and u_b were treated knowns for the facilitation of surface sound speed measurement, but this is not so practical in some cases. Note that there are a series of equivalent profiles that can be

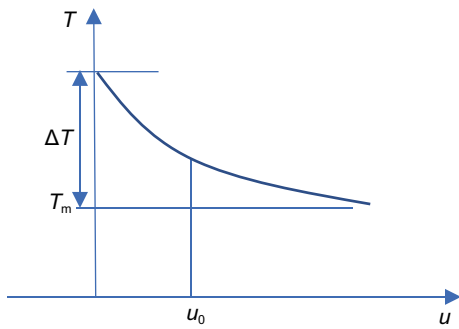


Fig. 1 Illustration on the empirical temperature profile

used to obtain almost the same positioning result (Sun et al., 2019; Zielinski & Geng, 1999), i.e., this is an ill-posed problem widely existed in nonlinear inversion. To obtain a meaningful solution, we should impose a prior information on \mathbf{p}_{BP} with a certain uncertainty, see the Table 3. For solving this problem, we however present a novel ESSP by Del Grosso sound speed formula with an ETP as follow

$$T_{ETP}(u, \mathbf{p}_{ETP}) = \boldsymbol{\tau} \mathbf{p}_{ETP} = T_m + \Delta T e^{-\frac{u}{u_0}} \quad (2)$$

where $\mathbf{p}_{ETP} = (T_m \ \Delta T)^T$ is an unknown parameter vector of ETP to be jointly estimated with the seafloor geodetic station coordinates, $\boldsymbol{\tau} = (T_m e^{-u/u_0})$ is the corresponding coefficient matrix, T_m represents the intermediate overmeasurement, ΔT represents the temperature difference between the sea-surface and sea-bottom, u_0 represents the depth of the thermocline, see Fig. 1. The u_0 and T_m can be statistically induced from the long-term

ocean environment observations and thereby we can impose prior constraints on the parameter estimation.

As shown in Fig. 1, the three parameters T_m , ΔT and u_0 to be estimated are the control parameters of the ETP shape. Note that the deep-sea bottom water temperature is generally very stable, for which it is convenient to impose a priori knowledge or constraint on the model parameter T_m . Besides, the deep-sea water temperature will decrease 1–2 °C per 1000 m, which might also be useful to characterize the ETP. Then, substituting ETP (2) and the average salinity $S = 35\text{‰}$ into the Del Grosso formula (Grosso, 1974; Wong & Zhu, 1995), we can establish an ESSP as

$$c_{ESSP}(u, \mathbf{p}_{ETP}) = \beta_C + \beta_P + \beta_T(\mathbf{p}_{ETP}) \quad (3)$$

where $c_{ESSP}(u, \mathbf{p}_{ETP})$ is ESSP,

$$\beta_C = C_c + C_{s(1)}S + C_{s(2)}S^2 \quad (4)$$

is a constant associated with the salinity S , C_c is the constant term in the Del Grosso formula,

$$\begin{aligned} \beta_P &= C_{s(2)p(2)}S^2P^2 + C_{p(1)}P + C_{p(2)}P^2 + C_{p(3)}P^3 \\ &= C_{p(1)}P + (C_{s(2)p(2)}S^2 + C_{p(2)})P^2 + C_{p(3)}P^3 \quad (5) \\ &= C_{p(1)}P + C_{d(1)}P^2 + C_{p(3)}P^3 \end{aligned}$$

is the sound speed variation associated with the pressure P which is recommended to use the Leroy’s formula as Leroy and Parthiot (1998)

$$P = 1.0052405(1 + 5.28 \times 10^{-3} \sin^2 \varphi)u + 2.36 \times 10^{-6}u^2 \quad (6)$$

where φ is the latitude,

$$\begin{aligned} \beta_T(\mathbf{p}_{ETP}) &= C_{t(1)}T_{ETP}(\mathbf{p}_{ETP}) + C_{t(2)}T_{ETP}^2(\mathbf{p}_{ETP}) \\ &\quad + C_{t(3)}T_{ETP}^3(\mathbf{p}_{ETP}) + C_{tp}PT_{ETP}(\mathbf{p}_{ETP}) \\ &\quad + C_{t(3)p}PT_{ETP}^3(\mathbf{p}_{ETP}) + C_{tp(2)}P^2T_{ETP}(\mathbf{p}_{ETP}) \\ &\quad + C_{t(2)p(2)}P^2T_{ETP}^2(\mathbf{p}_{ETP}) + C_{tp(3)}P^3T_{ETP}(\mathbf{p}_{ETP}) \\ &\quad + C_{st}ST_{ETP}(\mathbf{p}_{ETP}) + C_{st(2)}ST_{ETP}^2(\mathbf{p}_{ETP}) \\ &\quad + C_{stp}SPT_{ETP}(\mathbf{p}_{ETP}) + C_{s(2)tp}S^2PT_{ETP}(\mathbf{p}_{ETP}) \\ &= (C_{t(1)} + C_{st}S)T_{ETP}(\mathbf{p}_{ETP}) + ((C_{tp} + C_{stp}S + C_{s(2)tp}S^2)P \\ &\quad + C_{t(1)p(2)}P^2 + C_{t(1)p(3)}P^3)T_{ETP}(\mathbf{p}_{ETP}) \\ &\quad + (C_{st(2)}S + C_{t(2)})T_{ETP}^2(\mathbf{p}_{ETP}) + C_{t(2)p(2)}P^2T_{ETP}^2(\mathbf{p}_{ETP}) \\ &\quad + C_{t(3)}T_{ETP}^3(\mathbf{p}_{ETP}) + C_{t(3)p}PT_{ETP}^3(\mathbf{p}_{ETP}) \\ &= C_{d(2)}T_{ETP}(\mathbf{p}_{ETP}) + (C_{d(3)}P + C_{t(1)p(2)}P^2 + C_{t(1)p(3)}P^3)T_{ETP}(\mathbf{p}_{ETP}) \\ &\quad + C_{d(4)}T_{ETP}^2(\mathbf{p}_{ETP}) + C_{t(2)p(2)}P^2T_{ETP}^2(\mathbf{p}_{ETP}) \\ &\quad + C_{t(3)}T_{ETP}^3(\mathbf{p}_{ETP}) + C_{t(3)p}PT_{ETP}^3(\mathbf{p}_{ETP}) \end{aligned} \quad (7)$$

Table 1 ESSP coefficients

Coef	Value	Coef	Value
β_C	$1.449\,083\,403\,255 \times 10^3$	$C_{t(1)p(2)}$	$-0.159\,389\,5 \times 10^{-5}$
$C_{p(1)}$	0.156 059 2	$C_{t(1)p(3)}$	$0.522\,248\,3 \times 10^{-9}$
$C_{d(1)}$	$2.251\,941\,737\,5 \times 10^{-5}$	$C_{d(4)}$	-0.055 021 515 59
$C_{p(3)}$	$-0.883\,395\,9 \times 10^{-8}$	$C_{t(2)p(2)}$	$0.265\,617\,4 \times 10^{-7}$
$C_{d(2)}$	4.565 707 4	$C_{t(3)}$	$0.221\,649 \times 10^{-3}$
$C_{d(3)}$	$3.802\,021\,499\,999 \times 10^{-4}$	$C_{t(3)p}$	$-0.438\,361\,5 \times 10^{-6}$

is the sound speed variation determined by the water temperature T and the temperature-depth mixture terms.

With $S=35\%$, we can then figure out the coefficients of Eqs. (3), (4), (5), (7) and they are given in Table 1 for facilitating the calculation. Finally, for an arbitrary latitude specified we can figure out the ESSP by employing the data in Table 1.

As the proposed ESSP regards the sound speed variation with hydrostatic pressure of the water that implied in the Leroy’s formula and the water temperature’s exponential decaying characteristic with the depth that implied in the proposed empirical temperature profile, it is more meaningful and accurate to perform the SSP inversion result. We can also use other sound speed formulae to structure the ESSP complying with their applicable conditions, e.g., Wilson formula (Wilson, 1960) and Chen-Millero formula (Chen & Millero, 1977). In the following section, we will propose an optimization approach to determine the model parameters of ETP (2).

Two-level optimizations on ESSP

Overall Scheme

Next, we will conduct a joint estimation of ESSP parameters and the seafloor geodetic station coordinates by employing the 1st-level optimization as shown in Fig. 2, which is called as sound speed self-structured empirical SSP approach for its independence on the in-field SSP measurement.

As shown in Fig. 2, the 1st-level optimization is performed in the context of the ray-tracing positioning procedure while the 2nd-level one is performed by B-splines for characterizing acoustic delay caused by the sound speed variations relative to ESSP.

The 1st-level optimization

GNSS-A positioning is achieved by a combination of the sea-surface GNSS positioning with the precise acoustic round-trip time measurement from the sea-surface acoustic transducer to the seafloor acoustic transponder (Asada & Yabuki, 2006). Due to the horizontal density stratification of the ocean, the seafloor geodetic positioning generally uses the ray-tracing positioning model. For taking place of the high-cost in-field SSP measurement, we use ESSP $c_{ESSP}(u, \mathbf{p}_{ETP})$ to perform a joint estimation of \mathbf{p}_{ETP} and the seafloor geodetic coordinates. This time that the GNSS-A positioning model reads

$$T_{obs,i} = T_i(\mathbf{X}, c_{ESSP}(u, \mathbf{p}_{ETP})) + \varepsilon_{T,i} \tag{8}$$

where $T_{obs,i}$ is the i th round-trip time observation, \mathbf{X} is the seafloor transponder coordinate vector to

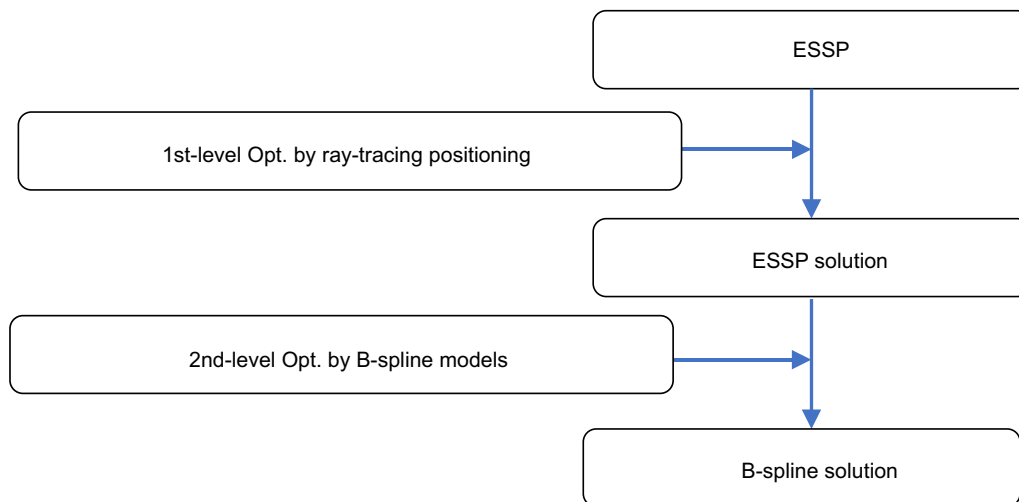


Fig. 2 Overall scheme of the two-level optimization

be estimated, $\varepsilon_{T,i}$ is the random error of observation. $T_i = T_{s,i} + T_{r,i}$ represents calculated the i th round-trip time,

$$T_{J,i} = \int_{u_X}^{u_x} \frac{1}{\cos \beta_i(u)} \frac{1}{c_{\text{ESSP}}(u, \mathbf{p}_{\text{ETP}})} du \quad J \in \{s, r\} \tag{9}$$

is one half of the round-trip travelling time calculated by the Two Dimensional (2D) ray-tracing model (Spiess, 1980), u_x, u_X are depths of the transducer and transponder, respectively. Note that, horizontal coordinates of transponder are implied in the incident angle $\beta_i(u)$ of the i th ray calculated by the inversion of the eigenray (Yang et al., 2021).

For n observations we have an over-determined vector-form observation equation $\mathbf{T}_{\text{obs}} = \mathbf{T}(X, c_{\text{ESSP}}(u, \mathbf{p}_{\text{ETP}})) + \boldsymbol{\varepsilon}_{\text{T}}$ solved by the nonlinear least squares (LS) criterion reads:

$$\min_{\mathbf{p}_{\text{ETP}}} g_1(X, \mathbf{p}_{\text{ETP}}) := \mathbf{V}^T(X, \mathbf{p}_{\text{ETP}}) \boldsymbol{\Sigma}_L^{-1} \mathbf{V}(X, \mathbf{p}_{\text{ETP}}) \tag{10}$$

where g_1 is the weighted sum of the squared residuals, $\mathbf{V}(X, \mathbf{p}_{\text{ETP}}) := \mathbf{T}_{\text{obs}} - \mathbf{T}(X, c_{\text{ESSP}}(u, \mathbf{p}_{\text{ETP}}))$ is the residual vector, and $\boldsymbol{\Sigma}_L = \mathbf{P}^{-1} \sigma_0^2$ and σ_0^2 are the variance of observations and prior unit weight variance, respectively. $\mathbf{P} = \text{diag}(p_1, p_2, \dots, p_n)$ is the weight matrix of observations where $p_i = (\sin(e_i))^2$ is the weight of the i th observation and e_i is the corresponding elevation angle, respectively. Hereafter, we however adopt an equal weight matrix to simplify the discussion, i.e., $p_i = 1$. To obtain LS solution we get the following first-order partial derivatives of $g_1(X, \mathbf{p}_{\text{ETP}})$, that is

$$\mathbf{h}(X, \mathbf{p}_{\text{ETP}}) = \begin{pmatrix} \partial g_1 / \partial X \\ \partial g_1 / \partial \mathbf{p}_{\text{ETP}} \end{pmatrix} = \begin{pmatrix} \mathbf{A}^T(X) \boldsymbol{\Sigma}_L^{-1} \mathbf{V}(X, \mathbf{p}_{\text{ETP}}) \\ \mathbf{B}^T(\mathbf{p}_{\text{ETP}}) \boldsymbol{\Sigma}_L^{-1} \mathbf{V}(X, \mathbf{p}_{\text{ETP}}) \end{pmatrix} \tag{11}$$

where

$$\mathbf{A}(X) = \frac{\partial \mathbf{T}}{\partial X} = \begin{pmatrix} \sum_{J \in \{s,r\}} \frac{\partial T_{J,1}}{\partial X} \\ \sum_{J \in \{s,r\}} \frac{\partial T_{J,2}}{\partial X} \\ \vdots \\ \sum_{J \in \{s,r\}} \frac{\partial T_{J,n}}{\partial X} \end{pmatrix} = c_X^{-1} \begin{pmatrix} \sum_{J \in \{s,r\}} (\sin \alpha_{J,1} \sin \beta_{J,1} \cos \alpha_{J,1} \sin \beta_{J,1} \cos \beta_{J,1}) \\ \sum_{J \in \{s,r\}} (\sin \alpha_{J,2} \sin \beta_{J,2} \cos \alpha_{J,1} \sin \beta_{J,2} \cos \beta_{J,2}) \\ \vdots \\ \sum_{J \in \{s,r\}} (\sin \alpha_{J,n} \sin \beta_{J,n} \cos \alpha_{J,n} \sin \beta_{J,n} \cos \beta_{J,n}) \end{pmatrix} \tag{12}$$

is the Jacobian matrix of the nonlinear observation about the coordinate vector, c_X is the sound speed at the depth of the transponder, $\alpha_{J,i}, \beta_{J,i}$ are the azimuth angle and incident angle of the i th ray, respectively.

$$\mathbf{B}(\mathbf{p}_{\text{ETP}}) = \frac{\partial \mathbf{T}}{\partial \mathbf{p}_{\text{ETP}}} = \frac{\partial \mathbf{T}}{\partial c_{\text{ESSP}}} \frac{\partial c_{\text{ESSP}}}{\partial \mathbf{p}_{\text{ETP}}} \tag{13}$$

is the first-order derivative of the round-trip time \mathbf{T} about \mathbf{p}_{ETP} . $\mathbf{B}(X)$ is hardly analytically given but it can be numerically solved. Then, vanishing $\mathbf{h}(X, \mathbf{p}_{\text{ETP}})$, i.e., we have

$$\begin{cases} \mathbf{A}^T(X) \boldsymbol{\Sigma}_L^{-1} \mathbf{V}(X, \mathbf{p}_{\text{ETP}}) = 0 \\ \mathbf{B}^T(\mathbf{p}_{\text{ETP}}) \boldsymbol{\Sigma}_L^{-1} \mathbf{V}(X, \mathbf{p}_{\text{ETP}}) = 0 \end{cases} \tag{14}$$

that can be used to obtain the LS solution. With initial values $X_0, \mathbf{p}_{\text{ETP}(0)}$, if $g_1''(X_0, \mathbf{p}_{\text{ETP}(0)})$ is positively defined, then LS solution can be locally solved by Newton's method with the second-order partial derivative of $g_1(X, \mathbf{p}_{\text{ETP}})$, that reads (Xue et al., 2014):

$$\begin{pmatrix} X_{k+1} \\ \mathbf{p}_{\text{ETP},k+1} \end{pmatrix} = \begin{pmatrix} X_k \\ \mathbf{p}_{\text{ETP},k} \end{pmatrix} + \left(\begin{matrix} \mathbf{A}_k^T \boldsymbol{\Sigma}_L^{-1} \mathbf{A}_k + \boldsymbol{\Gamma}_X & \mathbf{A}_k^T \boldsymbol{\Sigma}_L^{-1} \mathbf{B}_k \\ \mathbf{B}_k^T \boldsymbol{\Sigma}_L^{-1} \mathbf{A}_k & \mathbf{B}_k^T \boldsymbol{\Sigma}_L^{-1} \mathbf{B}_k + \boldsymbol{\Gamma}_p \end{matrix} \right)^{-1} \begin{pmatrix} \mathbf{A}_k^T \boldsymbol{\Sigma}_L^{-1} \mathbf{V}_k \\ \mathbf{B}_k^T \boldsymbol{\Sigma}_L^{-1} \mathbf{V}_k \end{pmatrix} \tag{15}$$

where $\mathbf{A}_k := \mathbf{A}(X_k)$, $\mathbf{B}_k := \mathbf{B}(\mathbf{p}_{\text{ETP},k})$, $\mathbf{V}_k := \mathbf{V}(X_k, \mathbf{p}_{\text{ETP},k})$ and k is the iteration index,

$$\boldsymbol{\Gamma}_X = \sum_{i=1}^n V_i(X, \mathbf{p}_{\text{ETP}}) p_i \sigma_0^{-2} \mathbf{S}_i(X) \tag{16}$$

in which $\mathbf{S}_i(X) = \partial \mathbf{a}_i^T(X) / \partial X$ is the first-order derivative of the i th row $\mathbf{a}_i(X)$ of $\mathbf{A}(X)$, i.e., the Hessian matrix of the round-trip time $T_i(X)$ about X ,

$$\boldsymbol{\Gamma}_p = \sum_{i=1}^n V_i(X, \mathbf{p}_{\text{ETP}}) p_i \sigma_0^{-2} \mathbf{Q}_i(\mathbf{p}_{\text{ETP}}) \tag{17}$$

in which $\mathbf{Q}_i(\mathbf{p}_{\text{ETP}}) = \partial \mathbf{b}_i^T(\mathbf{p}_{\text{ETP}}) / \partial \mathbf{p}_{\text{ETP}}$ is the first-order derivative of the i th row $\mathbf{b}_i(X)$ of $\mathbf{B}(\mathbf{p}_{\text{ETP}})$, i.e., the

Hessian matrix of the round-trip time $T_i(\mathbf{p}_{ETP})$ about \mathbf{p}_{ETP} . Note that, $\mathbf{\Gamma}_X$ and $\mathbf{\Gamma}_p$ can be ignored for long-distance or small-residual cases, and at this time we recommend using Gauss–Newton iterative formula as

$$\begin{aligned} \begin{pmatrix} X_{k+1} \\ \mathbf{p}_{ETP,k+1} \end{pmatrix} &= \begin{pmatrix} X_k \\ \mathbf{p}_{ETP,k} \end{pmatrix} \\ &+ \begin{pmatrix} A_k^T \Sigma_L^{-1} A_k & A_k^T \Sigma_L^{-1} B_k \\ B_k^T \Sigma_L^{-1} A_k & B_k^T \Sigma_L^{-1} B_k \end{pmatrix}^{-1} \\ &\begin{pmatrix} A_k^T \Sigma_L^{-1} V_k \\ B_k^T \Sigma_L^{-1} V_k \end{pmatrix} \end{aligned} \quad (18)$$

which is recommended to be terminated under the condition $\max_{i=1,2,\dots,S} (\|X_{i,k+1} - X_{i,k}\|) < \delta$ where δ is a sufficient small positive value, i is the index of the S seafloor geodetic stations. It is generally necessary to introduce a certain number of constraints on partial parameters to stabilize the iteration or to obtain a meaningful solution.

Next, we impose a priori constraints on \mathbf{p}_{ETP} . The first a priori constraint can be structured by the temperature stability of the seawater-bottom, that is

$$T_b = T_{ETP}(u_X, \mathbf{p}_{ETP}) + \varepsilon_b \quad (19)$$

where u_X is the depth of the seafloor geodetic station, the error ε_b represents the uncertainty of the a priori seawater-bottom temperature. Note that because deep-sea temperature is generally quite stable, the

$$\begin{aligned} \begin{pmatrix} X_{k+1} \\ \mathbf{p}_{ETP,k+1} \end{pmatrix} &= \begin{pmatrix} X_k \\ \mathbf{p}_{ETP,k} \end{pmatrix} + \begin{pmatrix} A_k^T \Sigma_L^{-1} A_k & A_k^T \Sigma_L^{-1} B_k \\ B_k^T \Sigma_L^{-1} A_k & B_k^T \Sigma_L^{-1} B_k \end{pmatrix}^{-1} \\ &\begin{pmatrix} A_k^T \Sigma_L^{-1} V_k \\ B_k^T \Sigma_L^{-1} V_k + (\Sigma_T^b)^{-1}(T_b - \tau \mathbf{p}_{ETP,k}) + (\Sigma_p^{ETP})^{-1}(\mathbf{p}_{ETP(0)} - \mathbf{p}_{ETP,k}) \end{pmatrix} \end{aligned} \quad (23)$$

average temperature of the seawater bottom can be easily obtained by global ocean environment observations.

Let Σ_T^b be the variance of T_b , we can structure the following LS criterion

$$\begin{aligned} \min g_1(\mathbf{Z}) &= \mathbf{V}^T(\mathbf{X}, \mathbf{p}_{ETP}) \Sigma_L^{-1} \mathbf{V}(\mathbf{X}, \mathbf{p}_{ETP}) \\ &+ (T_b - \tau \mathbf{p}_{ETP})^T (\Sigma_T^b)^{-1} (T_b - \tau \mathbf{p}_{ETP}) \end{aligned} \quad (20)$$

where $\mathbf{Z} = (\mathbf{X}^T \ \mathbf{p}_{ETP}^T)^T$ is the parameter vector to be estimated. Omitting the deduction, we can obtain the Gauss–Newton iterative formula as

$$\begin{aligned} \begin{pmatrix} X_{k+1} \\ \mathbf{p}_{ETP,k+1} \end{pmatrix} &= \begin{pmatrix} X_k \\ \mathbf{p}_{ETP,k} \end{pmatrix} + \begin{pmatrix} A_k^T \Sigma_L^{-1} A_k & A_k^T \Sigma_L^{-1} B_k \\ B_k^T \Sigma_L^{-1} A_k & B_k^T \Sigma_L^{-1} B_k + \tau^T (\Sigma_T^b)^{-1} \tau \end{pmatrix}^{-1} \\ &\begin{pmatrix} A_k^T \Sigma_L^{-1} V_k \\ B_k^T \Sigma_L^{-1} V_k + (\Sigma_T^b)^{-1}(T_b - \tau \mathbf{p}_{ETP,k}) \end{pmatrix} \end{aligned} \quad (21)$$

which is recommended to use the same termination condition. It is generally hard to obtain a global or meaningful solution of the problem without an effective initial value.

For most cases an arbitrary guess value of the unknown \mathbf{p}_{ETP} is sufficient to start the iteration, but we still recommend using a coarse grid search approach to obtain a robust initial value. Let $\mathbf{p}_{ETP(0)}$ and Σ_p^{ETP} be the initial value and the variance of \mathbf{p}_{ETP} , respectively, at this time we can structure the following LS criterion

$$\begin{aligned} \min g_1(\mathbf{Z}) &= \mathbf{V}^T(\mathbf{X}, \mathbf{p}_{ETP}) \Sigma_L^{-1} \mathbf{V}(\mathbf{X}, \mathbf{p}_{ETP}) \\ &+ (T_b - \tau \mathbf{p}_{ETP})^T (\Sigma_T^b)^{-1} \\ &(T_b - \tau \mathbf{p}_{ETP}) \\ &+ (\mathbf{p}_{ETP(0)} - \mathbf{p}_{ETP})^T (\Sigma_p^{ETP})^{-1} \\ &(\mathbf{p}_{ETP(0)} - \mathbf{p}_{ETP}) \end{aligned} \quad (22)$$

Omitting the deduction, we can write out the Gauss–Newton iterative formula as

The sea-surface temperature has a great fluctuation throughout the year, and thereby we recommend a very loose constraint on the parameter ΔT .

It is notable that Newton-type methods are of local convergence and may seriously suffer from ill-posedness of the problem, e.g., the non-uniqueness of the nonlinear parameter u_0 , and therefore it is recommended to be found out by a grid search method. In fact, the LS solution $\hat{\mathbf{Z}}$ of (23) can be treated as a function about the variable u_0 because of $\tau(u_0) = (T_m \ e^{-u/u_0})$ and it is denote as $\hat{\mathbf{Z}}(u_0)$.

The algorithm is given in Fig. 3.

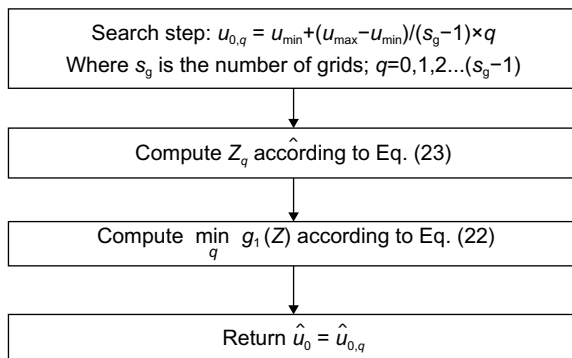


Fig. 3 1st-level optimization algorithm

Note that $T_m, \Delta T$ are linear parameters for (2) but they are nonlinear parameters both for (3) and (8), and therefore must be iteratively solved.

The 2nd-level optimization

Next, we will take the ESSP $c_{ESSP}(u, \mathbf{p}_{ETP})$ derived from the 1st-level optimization as a RSSP $c_0(u)$ to conduct the precise positioning. Regarding the N and E direction variations and temporal variation of the sound speed, we can express the Four Dimensional (4D) SSF $c(n, e, u, t)$ to be the form as

$$c(n, e, u, t) = c_0(u) + k_t(u, t)t + k_n(u, t)n + k_e(u, t)e \tag{24}$$

where $c_0(u) := c_{ESSP}(u, \mathbf{p}_{ETP})$ is the ESSP obtained from the 1st-level optimization, $k_n(u, t), k_e(u, t), k_t(u, t)$ are sound speed gradients of the SSF relative to RSSP.

It is very familiar to the sound speed inversion in the 1st-level optimization that the spatiotemporal sound speed gradients can be jointly estimated with the sea-floor geodetic coordinates. With “Appendix 1” we can directly write out the positioning model regarding the three sound speed gradients, that is

$$T_{obs} = \int_{u_X}^{u_x} (\cos \beta(u))^{-1} c_0^{-1}(u) du - m_t Z_t(t, \mathbf{p}_t) - m_n Z_n(t, \mathbf{p}_n) - m_e Z_e(t, \mathbf{p}_e) - m_{n'} Z_{n'}(t, \mathbf{p}_{n'}) - m_{e'} Z_{e'}(t, \mathbf{p}_{e'}) + \varepsilon_T \tag{25}$$

where t is the travel time observation,

$$\begin{cases} m_t = (\cos z)^{-1} \\ m_n = (\cos z)^{-1} \tan z \cos \alpha \\ m_e = (\cos z)^{-1} \tan z \sin \alpha \\ m_{n'} = (\cos z)^{-1} \tan z' \cos \alpha' \\ m_{e'} = (\cos z)^{-1} \tan z' \sin \alpha' \end{cases} \tag{26}$$

is the mapping function, z and α are the zenith angle and azimuth angle of the sea-surface platform observed at the seafloor geodetic station, respectively; z' and α' are the zenith angle and azimuth angle observed at the seafloor geodetic network array center, respectively.

$$\begin{cases} Z_t(t) = \int_{u_X}^{u_x} \lambda^{-1}(u) \frac{t k_t(u, t)}{c_0^2(u)} du \\ Z_n(t) = \int_{u_X}^{u_x} \lambda^{-1}(u) \frac{k_n(u, t) u}{c_0^2(u)} du \\ Z_e(t) = \int_{u_X}^{u_x} \lambda^{-1}(u) \frac{k_e(u, t) u}{c_0^2(u)} du \\ Z_{n'}(t) = \int_{u_X}^{u_x} \lambda^{-1}(u) \frac{k_n(u, t) u_X}{c_0^2(u)} du \\ Z_{e'}(t) = \int_{u_X}^{u_x} \lambda^{-1}(u) \frac{k_e(u, t) u_X}{c_0^2(u)} du \end{cases} \tag{27}$$

are the five zenith delays, $\lambda(u) = (\cos z)^{-1} \cos(\beta(u))$ can be defined as the measure of the ray bending degree. To characterize the five time-varying zenith delay parameters $Z_K(t), K \in \{t, n, e, n', e'\}$, the following B-splines

$$Z_K(t, \mathbf{p}_K) = \sum_{q=0}^{Q_K} p_{K,q} \Phi_{K,q,k}(t) \quad K \in \{t, n, e, n', e'\} \tag{28}$$

are recommended, $\mathbf{p}_K = (p_{K,1}, p_{K,2}, \dots, p_{K,Q(K)})$ is the unknown model parameter vector to be estimated, $p_{K,q}$ is the coefficient of the q th k -degree B-spline basis function $\Phi_{K,q,k}(t)$. This indicates the observation time span is split into $L_j = (Q_j - k + 1)$ intervals of which the knots span is $S_K = S_{all}/L_j$ where S_{all} is the observation time span. If it is not especially specified, the subscript k will be omitted in the following discussion.

At this stage, considering the smooth nature of the physical ocean process signal, we can conduct a series of 2-order smooths on the sound speed variations, and therefore we can alternatively use the optimization criterion as follow

$$\min_{\mathbf{X}, \mathbf{p}_K} g(\mathbf{X}, \mathbf{p}_K) := \mathbf{V}^T(\mathbf{X}, \mathbf{p}_K) \mathbf{P} \mathbf{V}(\mathbf{X}, \mathbf{p}_K) + \sum_{K \in \{t, n, e, n', e'\}} \|Z_K''(t, \mathbf{p}_K)\|^2 \tag{29}$$

where $Z_K''(t, \mathbf{p}_K)$ is the second-order derivative of $Z_K(t, \mathbf{p}_K)$ about the time,

$$\|Z_K''(t, \mathbf{p}_K)\|^2 = \lambda_K^2 \int_{t_1}^{t_2} (Z_K''(t, \mathbf{p}_K))^2 dt \tag{30}$$

is the squared norm of the estimated signal $Z_K''(t, \mathbf{p}_K)$, where t_1 and t_2 are the starting time and end time of the observation, respectively, which is defined by the inner product $\langle f_i(t), f_j(t) \rangle = \int f_i(t) \lambda_K f_j(t) dt$ of $f_i(t)$ and $f_j(t)$, λ_K^2 is the scale factor of the space specified by the above inner produce, which can be defined as

$$\lambda_K^2 = \sigma_{0,K}^{-2} \tag{31}$$

where $\sigma_{0,K}^2$ represents the variance of the random signal $Z''_K(t, \mathbf{p}_K)$.

To connect the minimization (29) with the normal form (20) of LS with constraints, we can rewrite (30) into the form as

$$\|Z''_K(t, \mathbf{p}_K)\|^2 = (\mathbf{0}^T - \mathbf{p}_K^T)(\Sigma_p^K)^{-1}(\mathbf{0} - \mathbf{p}_K) \tag{32}$$

where

$$(\Sigma_p^K)^{-1} = \mathbf{P}_p^K \sigma_{0,K}^{-2} \tag{33}$$

of which

$$\mathbf{P}_p^K = \begin{pmatrix} (\Phi''_{K,1}(t), \Phi''_{K,1}(t)) & (\Phi''_{K,1}(t), \Phi''_{K,2}(t)) & \cdots & (\Phi''_{K,1}(t), \Phi''_{K,Q(K)}(t)) \\ (\Phi''_{K,2}(t), \Phi''_{K,1}(t)) & (\Phi''_{K,2}(t), \Phi''_{K,2}(t)) & \cdots & (\Phi''_{K,2}(t), \Phi''_{K,Q(K)}(t)) \\ \vdots & \vdots & \ddots & \vdots \\ (\Phi''_{K,Q(K)}(t), \Phi''_{K,1}(t)) & (\Phi''_{K,Q(K)}(t), \Phi''_{K,2}(t)) & \cdots & (\Phi''_{K,Q(K)}(t), \Phi''_{K,Q(K)}(t)) \end{pmatrix} \tag{34}$$

is the weight matrix. Then, Omitting the deduction, we can immediately write out the Gauss–Newton solution of (29). To save the space, we write the Gauss–Newton solution only with the first three zenith delays, that is

the fact the station has a linear motion trend with the tectonic movement of the plate (Fig. 4).

We take the GNSS-Acoustic Ranging combined POsitioning Solver (GARPOS V1.0.0) software output as an external reference solution to evaluate the propose models. The GARPOS software adopts the recommended default parameter settings.

1st-level optimization results

Prior temperatures from Argo observation

We collected Argo observations around MYGI within an area of 110,889 km², lying within the interval [(142.9167° ± 1.5°) E, (38.0833° ± 1.5°) N], from March 28, 2011 to June 15, 2020, see Fig. 5. It shows that the sea-

$$\begin{pmatrix} X_{k+1} \\ \mathbf{p}_{N,k+1} \\ \mathbf{p}_{E,k+1} \\ \mathbf{p}_{t,k+1} \end{pmatrix} = \begin{pmatrix} X_k \\ \mathbf{p}_{N,k} \\ \mathbf{p}_{E,k} \\ \mathbf{p}_{t,k} \end{pmatrix} + \begin{pmatrix} A_k^T \Sigma_L^{-1} A_k & A_k^T \Sigma_L^{-1} M_N & A_k^T \Sigma_L^{-1} M_E & A_k^T \Sigma_L^{-1} M_t \\ M_N^T \Sigma_L^{-1} A_k & M_N^T \Sigma_L^{-1} M_N + (\Sigma_p^N)^{-1} & M_N^T \Sigma_L^{-1} M_E & M_N^T \Sigma_L^{-1} M_t \\ M_E^T \Sigma_L^{-1} A_k & M_E^T \Sigma_L^{-1} M_N & M_E^T \Sigma_L^{-1} M_E + (\Sigma_p^E)^{-1} & M_E^T \Sigma_L^{-1} M_t \\ M_t^T \Sigma_L^{-1} A_k & M_t^T \Sigma_L^{-1} M_N & M_t^T \Sigma_L^{-1} M_E & M_t^T \Sigma_L^{-1} M_t + (\Sigma_p^t)^{-1} \end{pmatrix}^{-1} \begin{pmatrix} A_k^T \Sigma_L^{-1} V_k \\ M_N^T \Sigma_L^{-1} V_k - (\Sigma_p^N)^{-1} \mathbf{p}_{N,k} \\ M_E^T \Sigma_L^{-1} V_k - (\Sigma_p^E)^{-1} \mathbf{p}_{E,k} \\ M_t^T \Sigma_L^{-1} V_k - (\Sigma_p^t)^{-1} \mathbf{p}_{t,k} \end{pmatrix} \tag{35}$$

where M_K is the design matrix of the parameter \mathbf{p}_K . The above formula can be easily extended for estimating the five zenith delays. Note that hyperparameter $\sigma_{0,K}^2$ might be optimally determined by the cross-test method or AIC criterion, but hereafter we set them to be zeros.

Experiment results and tests

Experimental data

The test adopts Japanese seafloor geodetic network array MYGI to verify the proposed GNSS-A positioning models. The observation span of the opened MYGI station data is from 2011 to 2020, having 35 repeated observations. The long-term displacement time series solution facilitates the positioning accuracy verification based on

surface temperature has a very large fluctuation, but the seawater bottom temperature is very stable. It is also hard to precisely fix the thermocline depth which lies within the interval (300 m 500 m).

The depth of MYGI station plots about 1727.8 m. the probability distribution of seawater bottom temperature at this depth in Fig. 6. It shows that, the mean of the seawater bottom temperature is 2.15 °C and STD is 0.09 °C. Therefore, we adopt the 1st-level optimization parameter settings in Table 2. The same method is used to analyze the seawater bottom sound speed.

The parameter settings of 1st-level optimization on bilinear SSP are given in Table 3. We impose lose constraints on the surface sound speed and the two sound speed gradients. Like constraining the bottom water temperature of ESSP, the bottom sound speed is imposed with a tight constraint 1486.62 m/s with the STD 0.01 m/s.

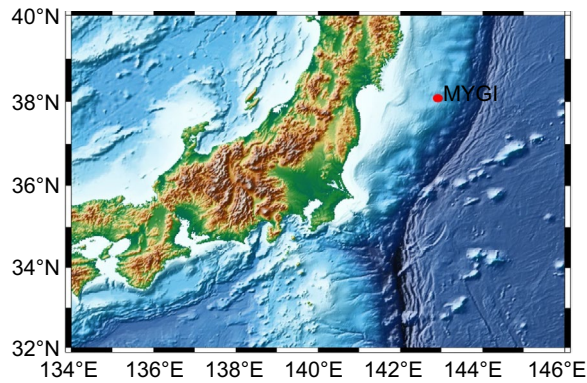


Fig. 4 MYGI station location

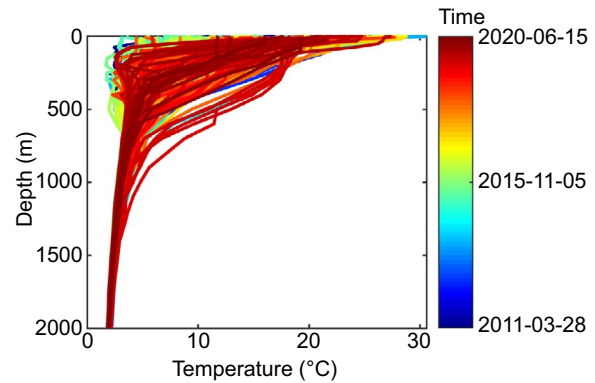


Fig. 5 MYGI surrounding Argo observations from 2011 to 2020

SSP inversion precision analysis

The SSP inversion results are compared with the in-field SSP and they are given in Fig. 7. It shows that the SSP inversions can overall characterize the shape of the in-field SSP, but it is hard to precisely fit the sea-surface sound speed. To precisely reflect the SSP inversion precision we adopt three piece-wise statistics, see Fig. 8.

Figure 8 shows that both for the bilinear SSP and ESSP the sound speed inversion precision increases with the depth, e.g., for the proposed ESSP, the mean bias and STD of the inversion sound speed in deepwater are 0.085 m/s and 2.448 m/s respectively, but those in the shallow water are up to 2.455 m/s and 10.862 m/s respectively. Table 4 shows that the inversion precision of proposed ESSP is overall better than that of the bilinear SSP even though the bilinear SSP has a relatively small bias for whole water column. Note that it is hard to avoid a bias in the inversion SSP relative to the in-field SSP.

Positioning precision analysis

We adopt the Argo SSP nearby MYGI station and the inversion SSPs to perform the positioning. Taking the positioning result based on the in-field SSP as a reference, we can then figure out the positioning errors caused by the substitutions of the in-field SSP and they given in Fig. 9. It shows that the Argo SSP solution has a relatively large positioning error especially in the vertical direction, but the solutions based on the inversion SSPs are almost same with each other.

The bias and STD of the positioning error series in Fig. 9 are figured out and they are given in Table 5. It shows that both the proposed ESSP solution and bilinear SSP can achieve decimeter-level-precision positioning, e.g., the positional error of the proposed ESSP solution for each coordinate component doesn't exceed 0.4 m, but there are biases 0.003 m and -0.016 m in *E* direction and *N* direction, respectively. The vertical bias of proposed

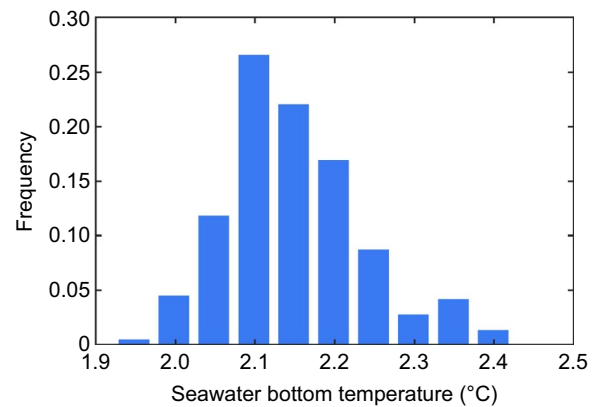


Fig. 6 Seawater temperature distribution at the depth 1727.8 m

Table 2 Parameter settings of 1st-level optimization on ESSP

Parameter	Value
Depth of the thermocline u_0	Searching range: (300 m 500 m), searching step: 25 m
Bottom temperature limitation T_m	2 °C with STD 1×10^5 °C
Bottom temperature T_b	2 °C with STD 0.1 °C
Temperature difference ΔT	10 °C with STD 10 °C

ESSP solution is smaller than that of the bilinear SSP solution and they are -0.219 m and -0.260 m, respectively, but their horizontal biases can be considered at the same order for centimeter-precision-level positioning. Although the bilinear SSP inversion precision is significantly lower than that the proposed ESSP, both the bilinear SSP solution and the proposed ESSP solution possess almost the same residual with the in-field SSP solution, see Fig. 10. This indicates that the two inversion SSPs are approximately equivalent to each other for the geodetic positioning application. This also shows that imposing a

Table 3 Parameter settings of 1st-level optimization on bilinear SSP

Parameter	Value
Surface sound speed v_s	1500 m/s with STD 5 m/s
Shallow-water sound speed gradient g_u	-0.1 with STD 100
Deep-water sound speed gradient g_d	0.01 with STD 100
Bottom sound speed	1486.62 m/s with STD 0.01 m/s

prior knowledge about the sound speed on the inversion is vitally important to obtain a meaningful SSP inversion solution.

2nd-level optimization results

We use the parameter settings in Table 6 for performing the 2nd-level optimization. Note that the positioning accuracy may be further improved by optimally selecting the knots span S_b , S_{NEU} and the smooth factor σ_K^{-2} .

The above empirical parameter settings listed in Table 6 will be further validated in following page.

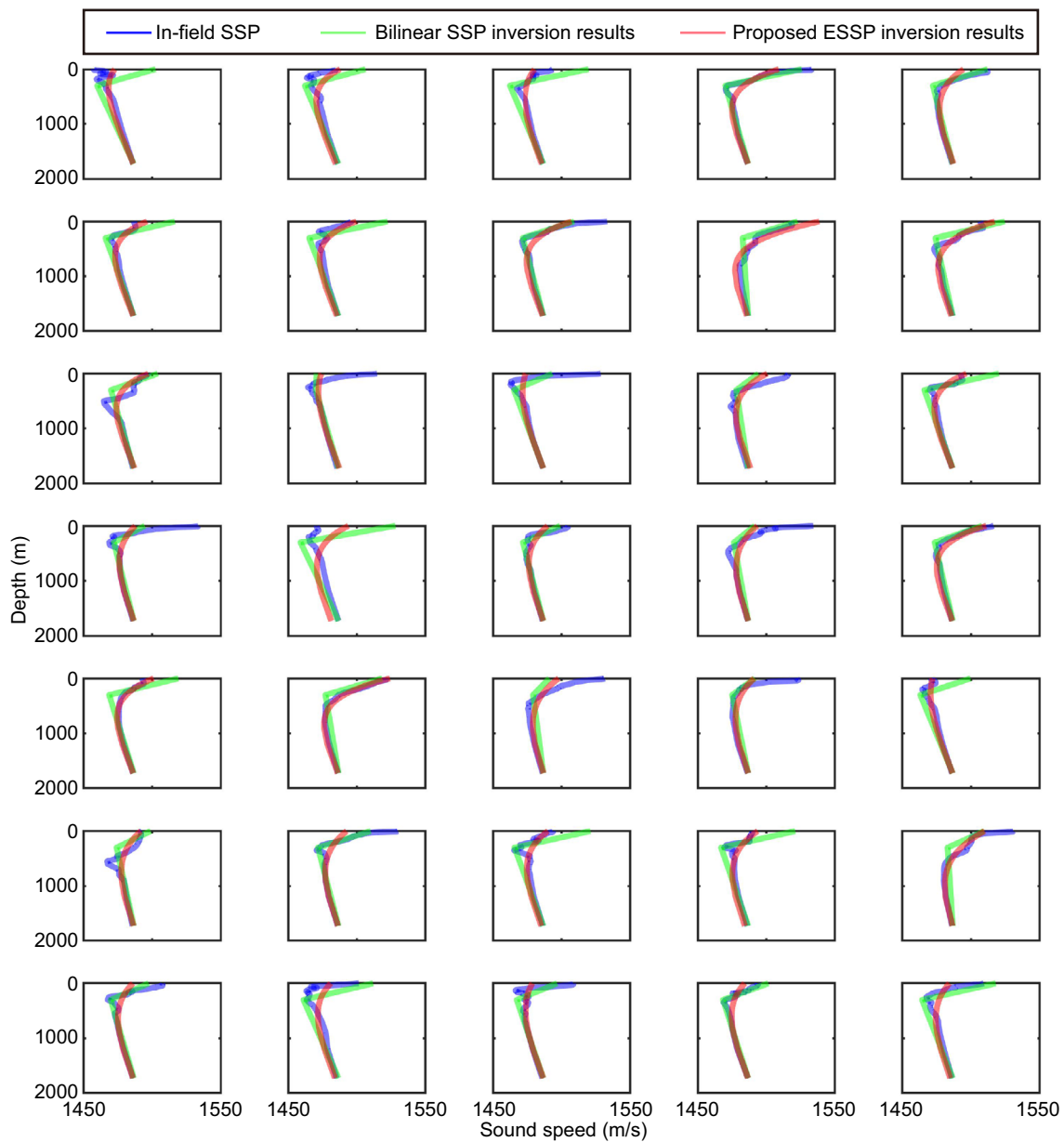


Fig. 7 SSP inversion results from 1st-level optimization

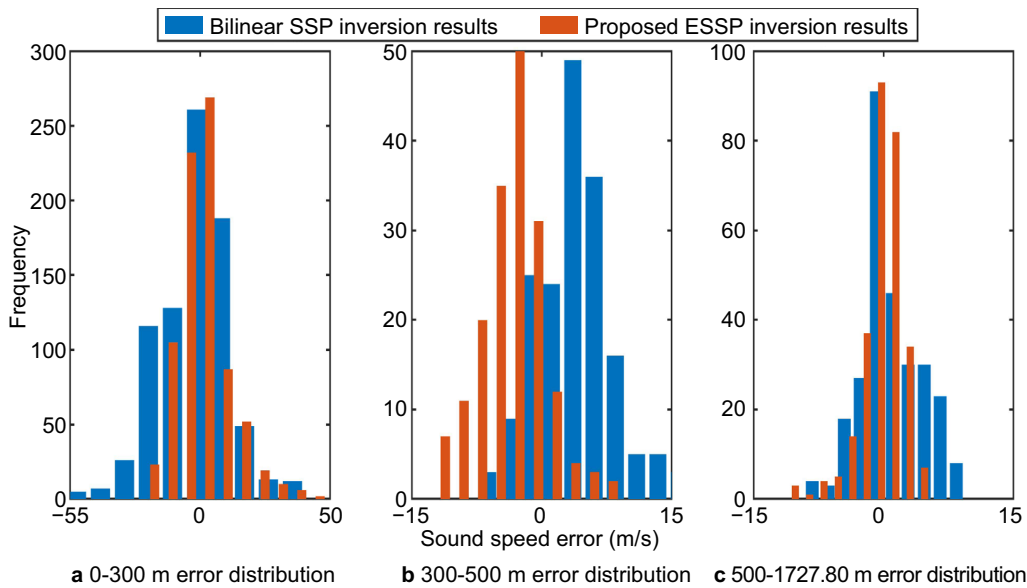


Fig. 8 Piece-wise statistics for SSP inversion precision

Table 4 Mean bias and STD of the inversion SSP

SSP depth range (m)	Mean bias from two methods		STD from two methods	
	Bilinear SSP (m/s)	ESSP (m/s)	Bilinear SSP (m/s)	ESSP (m/s)
0–1727.80	−1.540	1.413	12.652	9.226
0–300	−3.031	2.455	14.931	10.862
300–500	3.706	−3.132	4.344	3.723
500–1727.80	0.796	0.085	3.415	2.448

The positioning results based on the 2nd-level optimization are given in Fig. 11. It shows that the *E* and *N* coordinate biases existing in the 1st-level optimization have been removed at a great extent.

Table 7 shows that the horizontal precision of 2nd-level optimization for ESSP is better than 3 mm, while the vertical precision is better than 3 cm. The horizontal positioning accuracy of ESSP is very close to that of bilinear SSP, but vertical STD of ESSP solution is 0.0238 m which is significantly smaller than that 0.0433 m of bilinear SSP solution. Further considering the positioning error of the reference solution based on the in-field SSP, we can draw the conclusion that the proposed two-level optimization approach can achieve almost the same horizontal positioning precision with that based on in-field SSP. This conclusion becomes more solid when making a comparison among the 2nd-level optimization residuals of different SSP solutions as shown in Fig. 12. It also shows that the residuals are sharply shrunk after applying the 2nd optimization, compare to Fig. 9. A special attention on an

existing bias about 1 cm in the vertical direction needs to be paid in future studies.

Long-term displacement time series analysis

Let \bar{X}_j be the undetermined array geometry to perform the rigid-array fixed solution, $\Delta X^{(\kappa)}$ be the positional difference of the array center for κ th-epoch observation, and they can be determined by solving the equation as (Watanabe et al., 2020):

$$\begin{cases} X_j^{(\kappa)} = \delta_j^{(\kappa)} \bar{X}_j + \delta_j^{(\kappa)} \Delta X^{(\kappa)} & (j = 1, \dots, w; \kappa = 1, \dots, \eta) \\ 0 = \sum_{\kappa=1}^{\eta} \Delta X^{(\kappa)} \end{cases} \tag{36}$$

where, if the transponder j is used in κ th observation, $\delta_j^{(\kappa)} = 1$. In addition, $\delta_j^{(\kappa)} = 0$. where w and η are the number of transponders and epochs, respectively, and $X_j^{(\kappa)}$ denotes the transponders' position at the κ th-epoch.

The long-term displacement time series obtained by (36) is plotted in Fig. 13. The GARPOS solution time

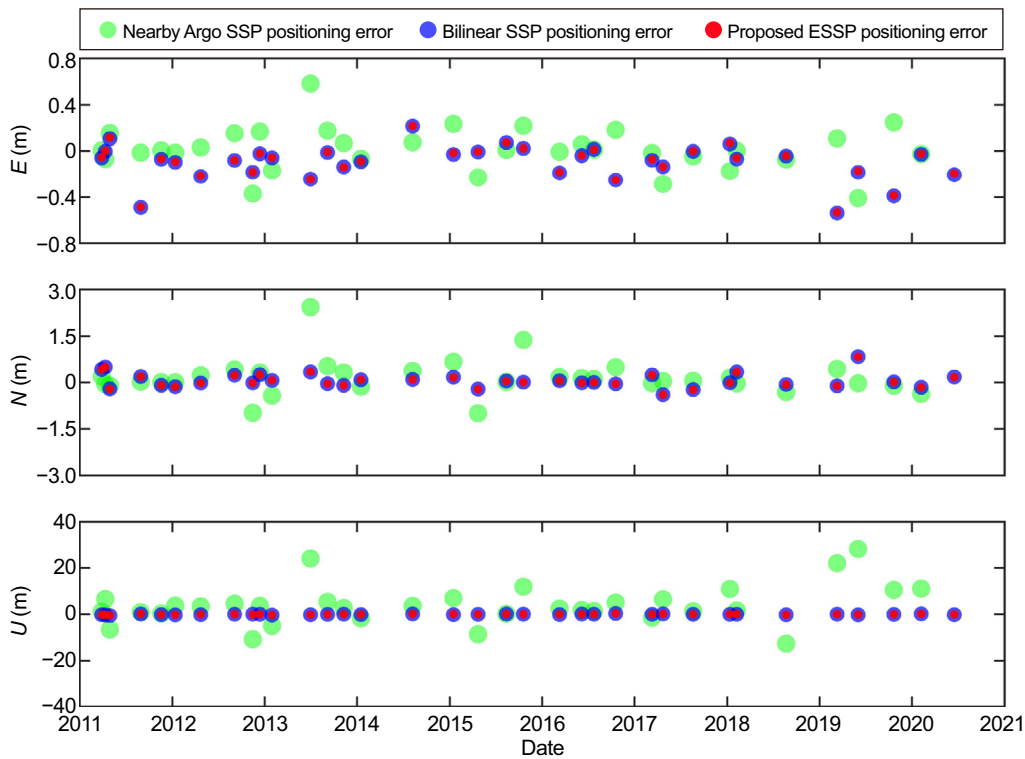


Fig. 9 Solutions of Argo SSP, bilinear SSP and ESSP

Table 5 Positioning error comparison of the solutions based on different SSPs

Index	Positioning errors of nearby Argo SSP in different directions (m)			Positioning errors of bilinear SSP in different directions (m)			Positioning errors of ESSP in different directions (m)		
	<i>E</i>	<i>N</i>	<i>U</i>	<i>E</i>	<i>N</i>	<i>U</i>	<i>E</i>	<i>N</i>	<i>U</i>
Accuracy mean bias	0.016	0.149	4.016	-0.001	-0.013	-0.260	0.003	-0.016	-0.219
Accuracy STD	0.189	0.587	8.748	0.018	0.025	0.353	0.019	0.024	0.355

series based on in-field SSP as an external reference is also plotted in Fig. 13 for conducting the comparison. Then, we can use the linear model $x(t) = x_0 + vt + e$ where x is the displacement time series and v is the velocity to fit the displacement time series to verify the proposed approach. The LS fitting residual as an estimation of the observation error e can be then used to evaluate the positioning precision.

Figure 13 shows that the proposed 2nd-level optimization approach can produce almost the same station movement trend as the GARPOS solutions, and more detailed information about the time series residuals is given in Table 8.

Table 8 shows that the largest difference among the station velocities along E, N, U directions is about 5.5 mm/a and it happens in the U direction. The horizontal displacement time series residual STDs of proposed models

are close to that of GARPOS model. The influence of the substitution of the in-field SSP with the self-structured ESSP on the station velocity estimation are 0.0, 0.4 and -1.4 mm/a in E, N, U directions, respectively, which can be ignored in applying GNSS-A to the seafloor geodesy in the current state of the art. We can draw almost the same conclusion for apply the bilinear SSP to the seafloor geodetic positioning. It is a very interesting but important that for seafloor geodetic positioning at centimeter precision and long-term tectonic displacement monitoring in-field SSP measurements might be unnecessary. However, as an extra product the SSP inversion should keep its physical meaning by imposing a prior knowledge, such as the hydrostatic pressure of the water and the water temperature's exponential decaying characteristic with the depth.

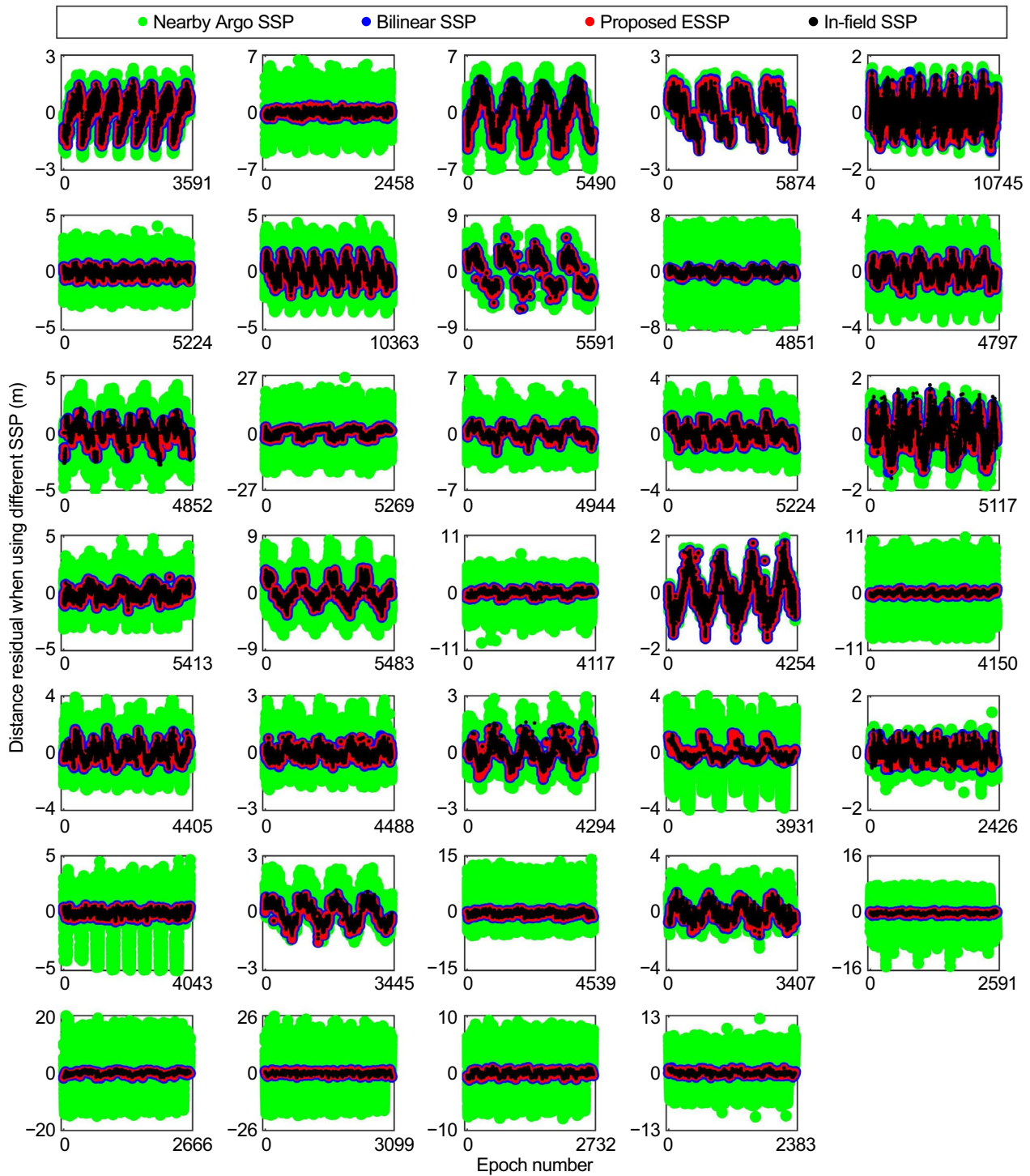


Fig. 10 1st-level optimization residuals of different SSP solutions

Remarks and conclusions

High-cost in-field SSP measurements have prevented GNSS-A from global seafloor geodesy, especially for real-time applications. The proposed self-structured SSP

(SSSP) approach is a useful way to facilitate GNSS-A for conducting the large-scale and even global seafloor geodetic positioning.

Table 6 Parameter settings for 2nd-level optimization

Parameter	Value
B-Spline degree k	3
B-Spline interval length S_t	15 min
B-Spline interval length S_{NEU}	35 min
Smooth factor $\sigma_K^{-2} = 0$	0

The overall shape of the in-field SSP can be characterized by the proposed three-parameter empirical temperature profile by performing a joint estimation of the three parameters with the seafloor geodetic coordinates. However, the global optimal solution of the thermocline depth parameter is hard to be obtained in the context of

the Gauss–Newton method because of its non-uniqueness and local convergence, and therefore the grid search method is recommended to be used. The seawater bottom temperature might also face with ill-posed problems, but fortunately the seawater bottom temperature prior constraint can be easily structured by the history ocean environment observations or by the current ocean temperature knowledge because of its stability.

The inaccuracy of the self-structured SSP can be almost completely absorbed by the proposed 2nd-level optimization such that it can achieve almost the same positioning result as that based on the in-field SSP. The influence of substituting the in-field SSP with the proposed SSSP on the horizontal positioning is less than 3 mm while that on the vertical positioning is better than 3cm in the STD

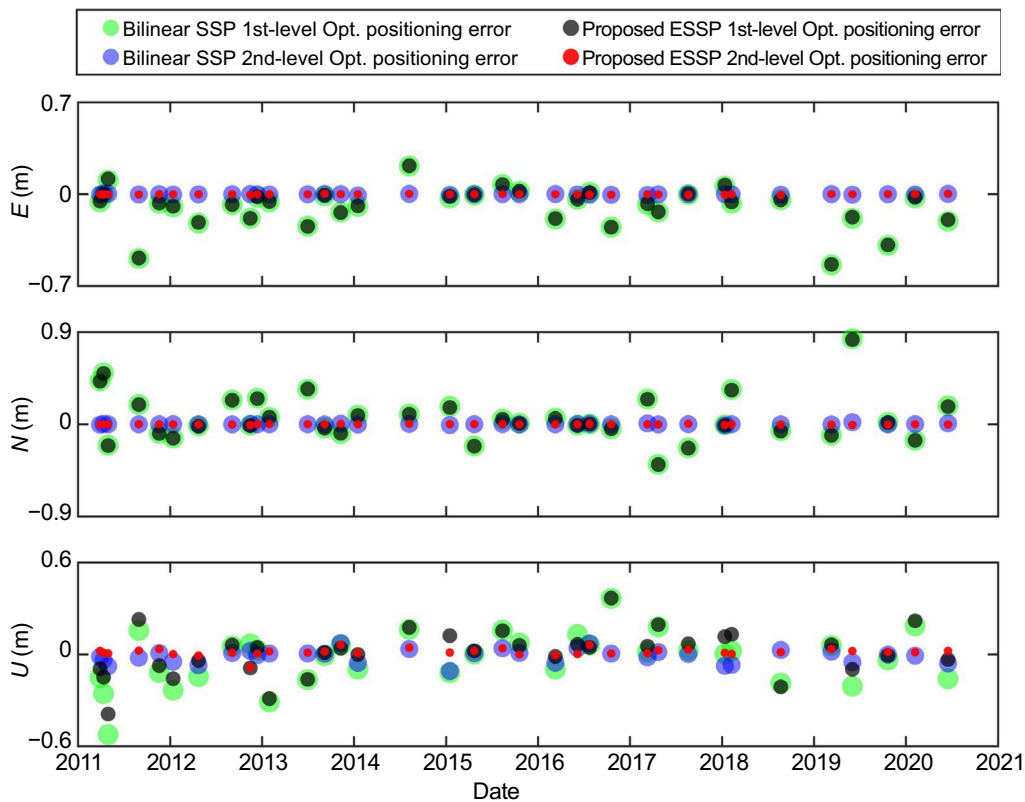


Fig. 11 Comparison of 1st-level and 2nd-level optimizations

Table 7 Accuracy comparison of 1st-level optimization and 2nd-level optimization

Index	Positioning errors of Bilinear SSP 2nd-level Opt in different directions (m)			Positioning errors of ESSP 2nd-level Opt in different directions (m)		
	E	N	U	E	N	U
Accuracy mean bias	-0.0006	0.0010	-0.0110	-0.0003	-0.0002	0.0148
Accuracy STD	0.0027	0.0049	0.0433	0.0021	0.0027	0.0238

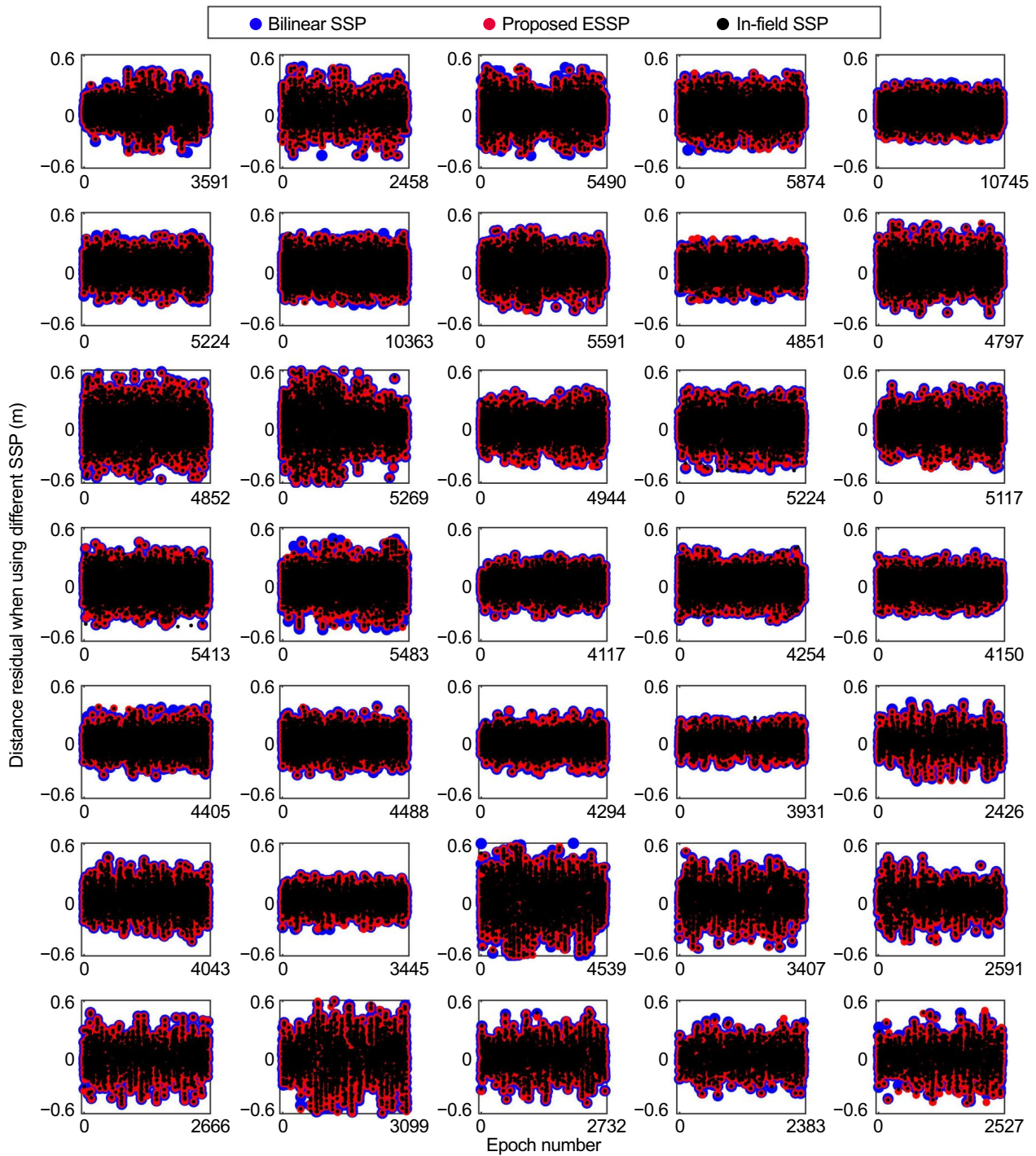


Fig. 12 2nd-level optimization residuals of different SSP solutions

sense. The influence of the substitution of the in-field SSP with the self-structured SSP on the station velocity estimation are further reduced to be omitted for applying GNSS-A to the seafloor geodesy in current state of

the art. Sound speed inversion accuracy of the proposed SSSP is more accurate than the bilinear SSP and this leads to a more accurate vertical positioning precision.

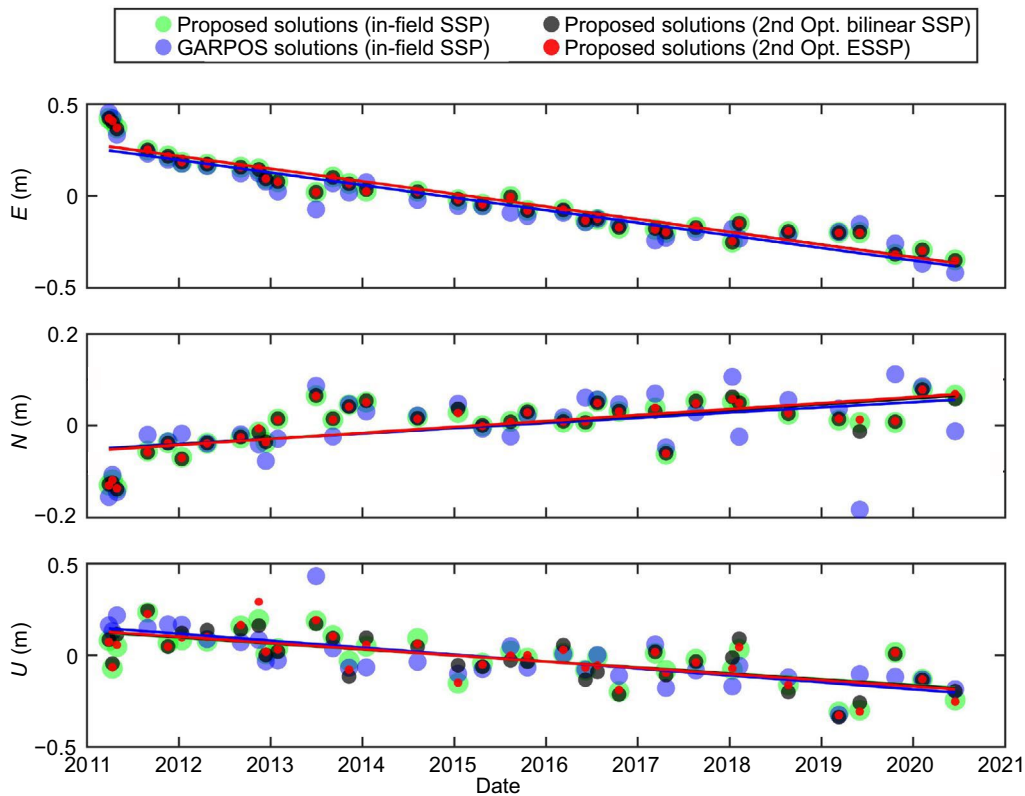


Fig. 13 GARPOS solution and the proposed 2nd-level optimization solution

Table 8 Displacement time series analysis results

Solutions	Station velocity from different solutions in different directions (m/a)			Residual STD from different solutions in different directions (m)		
	<i>E</i>	<i>N</i>	<i>U</i>	<i>E</i>	<i>N</i>	<i>U</i>
ESSP 2nd-level Opt.	-0.0689	0.0130	-0.0336	0.0591	0.0410	0.1013
Bilinear SSP 2nd-level Opt.	-0.0687	0.0125	-0.0327	0.0583	0.0431	0.0967
Delay model (in-field SSP)	-0.0689	0.0126	-0.0322	0.0593	0.0417	0.0942
GARPOS model (in-field SSP)	-0.0684	0.0114	-0.0377	0.0763	0.0638	0.0964

Appendix 1: Seafloor geodetic positioning models with five acoustic zenith delays

As shown in Fig. 14, without loss of generality, let the origin of NEU coordinate system be the centroid of the seafloor geodetic network array, let the RSSP $c_0(u)$ be at $(n_0 = 0, e_0 = 0, t_0 = 0)$, the first-order Taylor series expansion of SSF $c(n, e, u, t)$ at $(n_0 = 0, e_0 = 0, t_0 = 0)$ reads

$$c(n, e, u, t) = c_0(u) + k_n(u, t)n + k_e(u, t)e + k_t(u, t)t \tag{37}$$

where $k_n(u, t) := k_n(0, 0, u, t)$, $k_e(u, t) := k_e(0, 0, u, t)$, $k_t(u, t) := k_t(0, 0, u, t)$ are the partial derivatives about

the variable n, e and t , respectively, which represent the gradients of SSF.

As shown in Fig. 14, let α' and z' are the azimuth angle and zenith angle of the surface transducer position \mathbf{x} , \mathbf{X} is the seafloor transponder coordinate vector to be estimated, u_X be the depth of the seafloor geodetic station, then SSP at the position \mathbf{x} can be expressed as

$$\begin{aligned} c'_0(u, t) &= c_0(u) + k_t(u, t)t + n_x k_n(u, t) + e_x k_e(u, t) \\ &= c_0(u) + k_t(u, t)t + u_X \tan(z') \\ &\quad (\cos(\alpha')k_n(u, t) + \sin(\alpha')k_e(u, t)) \end{aligned} \tag{38}$$

The acoustic range signal travelling time is determined by the SSP along the ray. With SSP $c'_0(u, t)$ at the surface transducer position, we can figure out SSP along the ray. The horizontal gradient of SSF is very small and therefore the sound speed along the ray can be approximated by that along the Line of Sight (LOS). Then, let α and z are the azimuth angle and zenith angle of the ray observed at the sea-floor transponder position X , at arbitrary depth u , we have

$$c(LOS) = c'_0(u, t) + u \tan(z)(\cos(\alpha)k_n(u, t) + \sin(\alpha)k_e(u, t)) \tag{39}$$

For approximating the ray travelling time function $T = \int_L c^{-1}(L)ds$ where L is the ray trajectory, with the Taylor series approximation $(y + dy)^{-1} = y^{-1} - y^{-2}dy$ we have

$$\begin{aligned} T &= \int_L c^{-1}(L)ds \approx \int_L c^{-1}(LOS)ds \\ &= \int_{u_X}^{u_x} (\cos \beta(u))^{-1} c^{-1}(LOS)du \\ &\approx \int_{u_X}^{u_x} (\cos \beta(u))^{-1} c_0^{-1}(u)du - D_t(t) - \tan(z)(\cos(\alpha)D_n(t) + \sin(\alpha)D_e(t)) \\ &\quad - \tan(z')(\cos(\alpha')D_{n'}(t) + \sin(\alpha')D_{e'}(t)) \end{aligned} \tag{40}$$

where

$$\begin{cases} D_t(t) = \int_{u_X}^{u_x} \frac{1}{\cos \beta(u)} \frac{tk_t(u, t)}{c_0^2(u)} du \\ D_n(t) = \int_{u_X}^{u_x} \frac{1}{\cos \beta(u)} \frac{uk_n(u, t)}{c_0^2(u)} du \\ D_e(t) = \int_{u_X}^{u_x} \frac{1}{\cos \beta(u)} \frac{uk_e(u, t)}{c_0^2(u)} du \\ D_{n'}(t) = \int_{u_X}^{u_x} \frac{1}{\cos \beta(u)} \frac{u_X k_n(u, t)}{c_0^2(u)} du \\ D_{e'}(t) = \int_{u_X}^{u_x} \frac{1}{\cos \beta(u)} \frac{u_X k_e(u, t)}{c_0^2(u)} du \end{cases} \tag{41}$$

are the acoustic delays along LOS. To counterbalance the ray incident angle $\beta(u)$ involved in (41), introducing the azimuthal angle z and then we can rewrite the model (40) into the form as follow

$$\begin{aligned} T_{\text{obs}} &= \int_{u_X}^{u_x} (\cos \beta(u))^{-1} c_0^{-1}(u)du - m_t Z_t(t) \\ &\quad - m_n Z_n(t) - m_e Z_e(t) - m_{n'} Z_{n'}(t) - m_{e'} Z_{e'}(t) + \varepsilon_T \end{aligned} \tag{42}$$

where T_{obs} is the observed value of round-trip time, ε_T is the random error of observation.

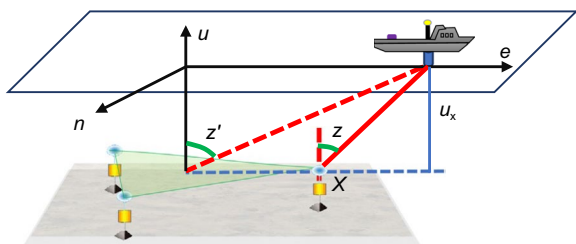


Fig. 14 Seafloor geodetic network geometry

$$\begin{cases} m_t = (\cos z)^{-1} \\ m_n = (\cos z)^{-1} \tan z \cos \alpha \\ m_e = (\cos z)^{-1} \tan z \sin \alpha \\ m_{n'} = (\cos z)^{-1} \tan z' \cos \alpha' \\ m_{e'} = (\cos z)^{-1} \tan z' \sin \alpha' \end{cases} \tag{43}$$

is the zenithal mapping function,

$$\begin{cases} Z_t(t) = \int_{u_X}^{u_x} \lambda^{-1}(u) \frac{tk_t(u, t)}{c_0^2(u)} du \\ Z_n(t) = \int_{u_X}^{u_x} \lambda^{-1}(u) \frac{k_n(u, t)u}{c_0^2(u)} du \\ Z_e(t) = \int_{u_X}^{u_x} \lambda^{-1}(u) \frac{k_e(u, t)u}{c_0^2(u)} du \\ Z_{n'}(t) = \int_{u_X}^{u_x} \lambda^{-1}(u) \frac{k_n(u, t)u_X}{c_0^2(u)} du \\ Z_{e'}(t) = \int_{u_X}^{u_x} \lambda^{-1}(u) \frac{k_e(u, t)u_X}{c_0^2(u)} du \end{cases} \tag{44}$$

where $\lambda(u) = (\cos z)^{-1} \cos \beta(u) \approx 1$ such that $Z_*(t)$ can represent the zenith delay unrelated to the time-varying of LOS. The above proposed model is different from the GARPOS model which adopts a default multiplicative compensation on the RSSP as

$$\begin{aligned}
 T(\mathbf{x}) &= \int_{u_x}^{u_x} \frac{1}{c(u, t)} ds \\
 &= \int_{u_x}^{u_x} \frac{1}{\Gamma(t)c_0(u)} ds \\
 &= \Gamma^{-1}(t) \int_{u_x}^{u_x} \frac{1}{c_0(u)} ds = \Gamma^{-1}(t)T_0(\mathbf{x})
 \end{aligned} \quad (45)$$

where $\Gamma(t)$ is a time-varying factor to characterize SSP variation, $T_0(\mathbf{x})$ is the travel time calculated by the RSSP, $T(\mathbf{x})$ is the travel time calculated by the time-varying SSP. To deal with the multiplicative compensation, we can follow the GARPOS approach taking logarithms on both sides of the observation $T_{\text{obs}} = \Gamma^{-1}(t)T_0(\mathbf{x}) + \varepsilon$, that is

$$\ln T_{\text{obs}} = \ln T_0(\mathbf{x}) + \ln \Gamma^{-1}(t) + \varepsilon' \quad (46)$$

Assuming $\Gamma^{-1}(t) = e^{\gamma(t)}$, we can have

$$\ln T_{\text{obs}} = \ln T_0(\mathbf{x}) + \gamma(t) + \varepsilon' \quad (47)$$

where ε' is the observation error vector, $\gamma(t)$ is the correction coefficient, which can be parameterized by a B-spline about the time. Further considering the horizontal gradient of sound speed, GARPOS finally adopts

$$\gamma(t) = \gamma_0(t) + \gamma_1(t) \cdot \mathbf{P}' + \gamma_2(t) \cdot \mathbf{X}' \quad (48)$$

where \mathbf{P}' is horizontal coordinate under the NEU coordinate system centered on specific original point which is the mean coordinates of transducer positions during the whole surveying session. \mathbf{X}' is horizontal coordinate under the NEU coordinate system centered on specific original point which is the mean coordinates of seafloor transponder array positions.

Acknowledgements

We are very grateful to Hydrographic and Oceanographic Department, Japan Coast Guard providing open seafloor geodetic data for this paper.

Author contributions

SQX proposed the main conception, and all the authors contributed to the study and experimental design. Material preparation, data collection and analysis were performed by SQX. The software code is programed by ZX and BJL. The first draft of the manuscript was written by SQX and then revised and commented on by BJL, YS, and JSL. All the authors read and approved the final manuscript.

Funding

This study was financially supported by National Natural Science Foundation of China (41931076), Laoshan Laboratory (LSKJ202205100, LSKJ202205105), and The Special Fund of Chinese Central Government for Basic Scientific Research Operations (AR2115).

Availability of data and materials

All experimental data can be obtained through the open-source website <https://www1.kaiho.mlit.go.jp/KOHO/chikaku/kaitei/sgs/datalist.html>

Declarations

Competing interests

All authors certify that they have no affiliations with or involvement in any organization or entity with any financial interest or non-financial interest in the subject matter or materials discussed in this manuscript.

Received: 8 March 2023 Accepted: 5 September 2023

Published online: 04 December 2023

References

- Asada, A., & Yabuki, T. (2006). Centimeter-level positioning on the seafloor. *Proceedings of the Japan Academy*, 77(1), 7–12.
- Bürgmann, R., & Chadwell, D. (2014). Seafloor geodesy. *Annual Review of Earth & Planetary Ences*, 42(1), 509–534.
- Chadwell, C. D., Spiess, F. N., Hildebrand, J. A., Young, L. E., Purcell, G. H., & Dragert, H. (1997). Sea floor strain measurement using GPS and acoustics. In J. Segawa, H. Fujimoto, & S. Okubo (Eds.), *Gravity, geoid and marine geodesy* (pp. 682–689). Springer.
- Chadwell, C. D., & Sweeney, A. D. (2010). Acoustic ray-trace equations for seafloor geodesy. *Marine Geodesy*, 33(2–3), 164–186.
- Chen, C., & Millero, F. J. (1977). Speed of sound in seawater at high pressures. *The Journal of the Acoustical Society of America*, 62(5), 1129–1135. <https://doi.org/10.1121/1.381646>
- Chen, G., & Herring, T. A. (1997). Effects of atmospheric azimuthal asymmetry on the analysis of space geodetic data. *Journal of Geophysical Research: Solid Earth*, 102(B9), 20489–20502.
- Chen, H. H. (2014). Travel-time approximation of acoustic ranging in GPS/Acoustic seafloor geodesy. *Ocean Engineering*, 84, 133–144.
- Del Grosso, V. A. (1974). New equation for the speed of sound in natural waters (with comparisons to other equations). *The Journal of the Acoustical Society of America*, 56(4), 1084–1091. <https://doi.org/10.1121/1.1903388>
- Fujita, M., Ishikawa, T., Mochizuki, M., Sato, M., Toyama, S., Katayama, M., et al. (2006). GPS/Acoustic seafloor geodetic observation: Method of data analysis and its application. *Earth, Planets and Space*, 58(3), 265–275.
- Fujita, M., Sato, M., & Yabuki, T. (2004). Development of seafloor positioning software using inverse method. *Report of Hydrographic and Oceanographic Researches*, 22, 50–56.
- Gagnon, K. L., & Chadwell, C. D. (2007). Relocation of a seafloor transponder—Sustaining the GPS-Acoustic technique. *Earth, Planets and Space*, 59(5), 327–336.
- Gagnon, K., Chadwell, C., & Norabuena, E. (2005). Measuring the onset of locking in the Peru–Chile trench with GPS and acoustic measurements. *Nature*, 434(7030), 205.
- Hayes, S., Mangum, L., Picaut, J., Sumi, A., & Takeuchi, K. (1991). TOGA-TAO: A moored array for real-time measurements in the tropical Pacific Ocean. *Bulletin of the American Meteorological Society*, 72(3), 339–347.
- Honsho, C., & Kido, M. (2017). Comprehensive analysis of traveltimes data collected through GPS-Acoustic observation of seafloor crustal movements. *Journal of Geophysical Research: Solid Earth*, 122(10), 8583–8599. <https://doi.org/10.1002/2017JB014733>
- Honsho, C., Kido, M., Tomita, F., & Uchida, N. (2019). Offshore postseismic deformation of the 2011 Tohoku Earthquake Revisited: Application of an improved GPS-Acoustic positioning method considering horizontal gradient of sound speed structure. *Journal of Geophysical Research: Solid Earth*, 124(6), 5990–6009.
- linuma, T., Kido, M., Ohta, Y., Fukuda, T., Tomita, F., & Ueki, I. (2021). GNSS-Acoustic observations of seafloor crustal deformation using a wave glider. *Frontiers in Earth Science*. <https://doi.org/10.3389/feart.2021.600946>
- Ikuta, R., Tadokoro, K., Ando, M., Okuda, T., Sugimoto, S., Takatani, K., et al. (2008). A new GPS-acoustic method for measuring ocean floor crustal

- deformation: Application to the Nankai Trough. *Journal of Geophysical Research*. <https://doi.org/10.1029/2006JB004875>
- Kido, M., Fujimoto, H., Miura, S., Osada, Y., Tsuka, K., & Tabei, T. (2006). Seafloor displacement at Kumano-nada caused by the 2004 off Kii Peninsula earthquakes, detected through repeated GPS/Acoustic surveys. *Earth, Planets and Space*, 58(7), 911.
- Kido, M., Osada, Y., & Fujimoto, H. (2008). Temporal variation of sound speed in ocean: A comparison between GPS/acoustic and in situ measurements. *Earth, Planets and Space*, 60(3), 229–234.
- Leroy, C. C., & Parthiot, F. (1998). Depth-pressure relationships in the oceans and seas. *The Journal of the Acoustical Society of America*, 103(3), 1346–1352. <https://doi.org/10.1121/1.421275>
- Matsumoto, Y., Fujita, M., & Ishikawa, T. (2008). *Development of multi-epoch method for determining seafloor station position*. <http://hdl.handle.net/1834/16415>
- Munk, W. H. (1974). Sound channel in an exponentially stratified ocean, with application to SOFAR. *The Journal of the Acoustical Society of America*, 55(2), 220–226. <https://doi.org/10.1121/1.1914492>
- Osada, Y., Fujimoto, H., Miura, S., Sweeney, A., Kanazawa, T., Nakao, S., et al. (2003). Estimation and correction for the effect of sound velocity variation on GPS/Acoustic seafloor positioning: An experiment off Hawaii Island. *Earth, Planets and Space*, 10(55), e17–e20. <https://doi.org/10.1186/BF03352464>
- Poutanen, M., & Rózsa, S. (2020). The Geodesist's handbook 2020. *Journal of Geodesy*, 94(11), 1–343. <https://doi.org/10.1007/s00190-020-01434-z>
- Roemmich, D., Johnson, G. C., Riser, S., Davis, R., Gilson, J., Owens, W. B., et al. (2009). The Argo program: Observing the global ocean with profiling floats. *Oceanography*, 22(2), 34–43.
- Sato, M., Fujita, M., Matsumoto, Y., Saito, H., Ishikawa, T., & Asakura, T. (2013). Improvement of GPS/acoustic seafloor positioning precision through controlling the ship's track line. *Journal of Geodesy*, 87(9), 825–842.
- Sato, M., Ishikawa, T., Ujihara, N., Yoshida, S., Fujita, M., Mochizuki, M., & Asada, A. (2011). Displacement above the hypocenter of the 2011 Tohoku-Oki earthquake. *Ence*, 332(6036), 1395.
- Spiess, F. (1980). Acoustic techniques for marine geodesy. *Marine Geodesy*, 4(1), 13–27.
- Spiess, F. (1985). Analysis of a possible sea floor strain measurement system. *Marine Geodesy*, 9(4), 385–398.
- Spiess, F. N., Chadwell, C. D., Hildebrand, J. A., Young, L. E., Purcell, G. H., & Dragert, H. (1998). Precise GPS/Acoustic positioning of seafloor reference points for tectonic studies. *Physics of the Earth & Planetary Interiors*, 108(2), 101–112.
- Stammer, D., Wunsch, C., Giering, R., Eckert, C., Heimbach, P., Marotzke, J., Adcroft, A., Hill, C. N., & Marshall, J. (2003). Volume, heat, and freshwater transports of the global ocean circulation 1993–2000, estimated from a general circulation model constrained by World Ocean Circulation Experiment (WOCE) data. *Journal of Geophysical Research: Oceans*, 108(C1), 7.
- Sun, W., Yin, X., & Zeng, A. (2019). The relationship between propagation time and sound velocity profile for positioning seafloor reference points. *Marine Geodesy*, 42(2), 186–200. <https://doi.org/10.1080/01490419.2019.1575938>
- Torge, W., & Müller, J. (2012). Geodesy. In *Geodesy*. de Gruyter.
- Watanabe, S., Ishikawa, T., Yokota, Y., & Nakamura, Y. (2020). GARPOS: Analysis software for the GNSS-A seafloor positioning with simultaneous estimation of sound speed structure. *Frontiers in Earth Science*, 8, 508. <https://doi.org/10.3389/feart.2020.597532>
- Wilson, W. D. (1960). Speed of sound in sea water as a function of temperature, pressure, and salinity. *The Journal of the Acoustical Society of America*, 32(6), 641–644. <https://doi.org/10.1121/1.1908167>
- Wilson, & Wayne, D. (1960). Equation for the speed of sound in sea water. *The Journal of the Acoustical Society of America*, 32(10), 1357–1357.
- Wong, G. S. K., & Zhu, S. (1995). Speed of sound in seawater as a function of salinity, temperature, and pressure. *The Journal of the Acoustical Society of America*, 97(3), 1732–1736. <https://doi.org/10.1121/1.413048>
- Wu, L., Chen, Z., Lin, X., & Liu, W. (2020). Building the integrated observational network of "Transparent Ocean." *Chinese Science Bulletin*, 65(25), 2654–2661.
- Xue, S., Yang, Y., & Dang, Y. (2014). A closed-form of Newton method for solving over-determined pseudo-distance equations. *Journal of Geodesy*, 88(5), 441–448. <https://doi.org/10.1007/s00190-014-0695-y>
- Yang, W., Xue, S., & Liu, Y. (2021). P-order secant method for rapidly solving the ray inverse problem of underwater acoustic positioning. *Marine Geodesy*. <https://doi.org/10.1080/01490419.2021.1992547>
- Yang, Y., Liu, Y., Sun, D., Xu, T., & Zeng, A. (2020). Seafloor geodetic network establishment and key technologies. *Science China Earth Science*, 8(63), 1188–1198.
- Yang, Y., & Qin, X. (2020). Resilient observation models for seafloor geodetic positioning. *Journal of Geodesy*, 95, 1–13.
- Yasuda, K., Tadokoro, K., Taniguchi, S., Kimura, H., & Matsuhiro, K. (2017). Inter-plate locking condition derived from seafloor geodetic observation in the shallowest subduction segment at the Central Nankai Trough, Japan. *Geophysical Research Letters*, 44(8), 3572–3579.
- Yokota, Y., Ishikawa, T., & Watanabe, S. (2019). Gradient field of undersea sound speed structure extracted from the GNSS-A oceanography: GNSS-A as a sensor for detecting sound speed gradient. *Marine Geophysical Research*, 40(4), 493–504. <https://doi.org/10.1007/s11001-018-9362-7>
- Yokota, Y., Watanabe, S., Ishikawa, T., & Nakamura, Y. (2022). Temporal change of km-scale underwater sound speed structure and GNSS-A positioning accuracy. *Earth and Space Science Open Archive*, 9, e2022EA002224.
- Zeng, L., Wang, D., Chen, J., Wang, W., & Chen, R. (2016). SCSPD14, a South China Sea physical oceanographic dataset derived from in situ measurements during 1919–2014. *Scientific Data*, 3(1), 1–13.
- Zhao, J., Liang, W., Ma, J., Liu, M., & Li, Y. (2022). A self-constraint underwater positioning method without the assistance of measured sound velocity profile. *Marine Geodesy*. <https://doi.org/10.1080/01490419.2022.2079778>
- Zielinski, A., & Geng, X. (1999). Precise multibeam acoustic bathymetry. *Marine Geodesy*, 22(3), 157–167.

Submit your manuscript to a SpringerOpen® journal and benefit from:

- Convenient online submission
- Rigorous peer review
- Open access: articles freely available online
- High visibility within the field
- Retaining the copyright to your article

Submit your next manuscript at ► [springeropen.com](https://www.springeropen.com)